Drug inhibition of redox factor-1 restores hypoxic-driven changes in Tuberous Sclerosis Complex 2-deficient cells

Jesse D. Champion [1], Kayleigh M. Dodd [1], Hilaire C. Lam [2], Mohammad A.M. Alzahrani [1], Sara Seifan [1], Ellie Rad [1], D. Oliver Scourfield [1], Melissa L. Fishel [3], Brian L. Calver [1], Ann Ager [4], Elizabeth P. Henske [2], David M. Davies [1,5], Mark R. Kelley [3] and Andrew R. Tee [1,*]

1. Division of Cancer and Genetics, Cardiff University, Heath Park, Cardiff CF14 4XN, UK; ChampionJD1@cardiff.ac.uk (J.D.C.); kayleigh.dodd@pharmagenesis.com (K.M.D.); AlzahraniMA1@cardiff.ac.uk (M.A.M.A.); SeifanS@cardiff.ac.uk (S.S.); RadE@cardiff.ac.uk (E.R.); ScourfieldDO@cardiff.ac.uk (D.O.S); CalverBL@cardiff.ac.uk (B.C.); DaviesDM@cardiff.ac.uk (D.M.D.)
2. Pulmonary and Critical Care Medicine, Department of Medicine, Brigham and Women's Hospital and Harvard Medical School, Boston, MA, USA; hclam@bwh.harvard.edu (H.C.L.); EHenske@bwh.harvard.edu (E.P.H.)
3. Herman B Wells Center for Pediatric Research, Indiana University School of Medicine, Indianapolis, Indiana, USA; mfishel@iu.edu (M.L.F.); mkelley@iu.edu (M.R.K.)
4. Division of Infection and Immunity, Cardiff University, Heath Park, Cardiff, CF14 4XN, UK; AgerA@cardiff.ac.uk (A.A.).
5. Department of Oncology, South West Wales Cancer Centre, Singleton Hospital, Swansea SA2 8QA, UK

Abstract: Therapies with mechanistic target of rapamycin complex 1 (mTORC1) inhibitors are not fully curative for Tuberous Sclerosis Complex (TSC) patients. Here we propose that some mTORC1-independent disease facets of TSC involve signaling through redox factor-1 (Ref-1). Ref-1 possesses redox signaling activity that stimulates the transcriptional activity of STAT3, NF-κB, and HIF-1α involved in inflammation, proliferation, angiogenesis and hypoxia, respectively. Here we demonstrate that redox signaling through Ref-1 contributes to metabolic transformation and tumor growth in TSC cell model systems. In TSC2-deficient cells, the clinically viable Ref-1 inhibitor, APX3330, was effective at blocking the hyperactivity of STAT3, NF-κB, and HIF-1α. While Ref-1 inhibitors do not inhibit mTORC1, they potently block cell invasion and vasculature mimicry. Of interest, we show that cell invasion and vasculature mimicry linked to Ref-1 redox signaling are not blocked by mTORC1 inhibitors. Metabolic profiling revealed that Ref-1 inhibitors alter metabolites associated with the glutathione antioxidant pathway as well as metabolites that are heavily dysregulated in TSC2-deficient cells involved in redox homeostasis. Therefore, this work presents Ref-1 and associated redox-regulated transcription factors, such as STAT3, NF-κB and HIF-1α, as potential therapeutic targets to treat TSC, where targeting these components would likely have additional benefits to just using mTORC1 inhibitors alone.

1. Introduction

Tuberous Sclerosis Complex (TSC) is a rare, autosomal dominant genetic condition caused by inactivating mutations in either the *TSC1* or *TSC2* genes. TSC patients are predisposed to benign tumors in multiple organs including the kidneys, skin, brain and heart (for reviews see [1-2]). Renal angiomyolipomas (AMLs) are the most frequent tumor, affecting approximately 80% of individuals with TSC and are a leading cause of morbidity in adulthood [3]. AMLs are highly vascularized and are composed of adipose and smooth muscle tissue. 90% of TSC patients also have at least one or more skin lesions that develop early in life. Facial angiofibromas are the most visible cutaneous feature of TSC that consist of fibrous tissue and blood vessels. Brain tumors are less frequent, but those that do occur can be associated with epilepsy. However, the formation of

brain tumors is not necessarily required for the development of epilepsy, where approximately 90% of TSC patients experience a seizure during their lifetime [4]. A proportion of seizures are resistant to anti-epileptic medications, making them difficult to control. Lymphangioleiomyomatosis (LAM), the pulmonary manifestation of TSC, affects almost exclusively women. TSC2-deficient LAM cells are believed to metastasize to the lungs, resulting in cystic lung destruction [5-6]. The pathophysiology of TSC is complex. While we have made significant forward progress, there is much we still need to understand. A deeper knowledge of the signaling mechanism defects that contribute to disease development is required and will allow development of better therapeutic strategies to treat the disease manifestations of TSC.

A key feature of TSC biology is the ability of the TSC1/TSC2 tumor suppressor protein complex to inhibit the mechanistic target of rapamycin complex 1 (mTORC1) signaling pathway involved in normal cell growth control. The small G protein, Ras homologue enriched in brain (Rheb) is negatively regulated by the GTPase activating protein (GAP) domain of TSC2 [7]. Loss of function *TSC1* or *TSC2* mutations constitutively switches Rheb to an active GTP-bound state that then aberrantly activates mTORC1, leading to metabolic transformation, uncontrolled tumor growth and encourages angiogenesis in hypoxic tissues (reviewed in [8]). The fundamental discovery of the Rheb-GAP tumor suppressor function of TSC2 positioned mTORC1 as a new drug target for the treatment of TSC. Consequently, rapamycin analogues (rapalogues) that inhibit mTORC1 are now clinically approved for the treatment of TSC. While improving quality of life for TSC patients, mTORC1 inhibition does not completely restore disease state. Both data from *in vitro* and clinical studies provide evidence that rapamycin is a cytostatic agent, and that cessation of therapy results in rebound and regrowth of TSC-tumors [9]. Further investigation into disease mechanisms of TSC is clearly required to reveal new drug targets and to advance therapeutic options.

While mTORC1 hyperactivation upon loss of *TSC1*/*TSC2* is a well-defined aspect of TSC, and mechanistically linked to tumor growth, we hypothesize that mTORC1-independent signaling mechanisms are also critically involved in the development of TSC. mTORC1-independent mechanisms might be involved in disease progression of TSC and LAM and could help explain why mTORC1 inhibitors only have a partial but stable response in TSC/LAM patients. We speculate that hypoxic signaling involved in angiogenesis and tumor growth becomes elevated in hypoxic TSC2-deficient tissue that is not dependent on mTORC1. Research has indicated that hypoxic signaling is a key driver of TSC [10-11], where loss of *TSC2* can pathologically promote expression of hypoxic inducible factor 1α (HIF-1α). HIF-1α regulation is multifaceted with multiple inputs that regulates its mRNA/protein expression, transcriptional activity and protein stability. We previously discovered that signal transducer and activator of transcription 3 (STAT3) functioned upstream of HIF-1α during hypoxia in TSC2-deficient cell models [11] required for HIF-1α mRNA gene expression. STAT3 has previously been shown to have an elevated level of Tyr705 phosphorylation in TSC2-deficient models [12-14]. Tyr705 phosphorylation is required for STAT3 activation and is regulated through tyrosine kinases, such as Janus kinase 2 (JAK2). Nuclear factor kappa-light-chain-enhancer of activated B cells (NF-κB) is another potential transcriptional input to HIF-1α [15] and to date has been understudied in TSC. HIF-1α activation leads to angiogenesis and tumor development, key features intrinsically linked to TSC. We postulate that TSC-associated pathology involves STAT3, NF-κB and HIF-1α.

We speculated that this STAT3, NF-κB and HIF-1α transcriptional signaling nexus might play a role in disease progression of TSC and LAM. Given that mTORC1 inhibitors are not fully restorative, we investigated another potential therapeutic strategy to restore disease features of TSC2-deficient cells. Through this work, we reveal a novel drug target for the therapy of TSC, called Ref-1 (also known as APE1 or APEX1). Ref-1 is involved in redox signaling pathways associated with cancer, including angiogenesis, proliferation, inflammation and hypoxia response (reviewed in [16]).

2. Materials and Methods

2.1. Antibodies and Biochemicals

Anti-TSC2, anti-STAT3 phospho-Ser727 and Tyr705, Ref-1, Rel-A phospho Ser365, anti-β-actin, VEGF-A, BNIP3, and anti-rpS6 phospho-Ser235/236 were obtained from Cell Signaling Technology (Danvers, MA USA). Anti-HIF-1α was purchased from BD Transduction Laboratories (Oxford, UK). Rapamycin, FL3331 and JSH23 were bought from Merck (Darmstadt, Germany), KU-0063794 was purchased from Chemquest Ltd (Cheshire, UK), while APX3330, APX2009, APX2011 and RN7-58 was obtained from Apexian Pharmaceuticals (Indianapolis, IN, USA). Unless stated otherwise, all other lab chemicals were obtained from Merck (Darmstadt, Germany).

2.2. Cell Culture, Transfection and Preparing Cell Lysates

Tsc2+/+*Tp53*−/− and *Tsc2*−/−*Tp53*−/− mouse embryonic fibroblasts (MEFs) was a kind gift from Prof. D Kwiatkowski (Harvard University, Boston, MA, USA) were cultured in Dulbecco's modified Eagle's medium supplemented with 10 % (v/v) foetal calf serum and 100 μ/ml penicillin streptomycin (Life Technologies/ThermoFisher Scientific, Waltham, MA, USA). Human TSC2-deficient cells angiomyolipomas AML 621-101 cells [17] were grown as above but were supplemented with 20 % (v/v) foetal calf serum. Transfections were carried out using JETPei transfection reagent (VWR International, Leicestershire, UK) as directed by the manufacturer's protocol. Drug were treated as indicated. Hypoxia experiments were set up in a Binder CB150 hypoxic chamber set at 1 % O_2 over-night (18 h). Cells were lysed directly in sample buffer (62.5 mM Tris–HCl (pH 7.6), 50 mM dithiothreitol, 2 % (w/v) sodium dodecyl sulphate , 10 % (w/v) glycerol, 0.1 % (w/v) bromophenol blue) and sonicated for 3 × 20 s cycles on full power (30 amplitude microns), heated at 95 °C for 10 min then centrifuged at 13,000 rpm for 8 min. Protein quantification was carried out using the Pierce 660 nm protein reagent (with ionic detergent compatibility reagent, bought from ThermoFisher Scientific, Waltham, MA, USA), before being subjected to western blotting. Immunoprecipitation of Ref-1: cell lysates were generated with lysis buffer (20 mm Tris, 135 mm NaCl, 5 % (v/v) glycerol, 50 mm NaF and 0.1 % (v/v) triton X-100, pH 7.5 supplemented with complete mini protease inhibitor cocktail (Roche Diagnostics Ltd. Burgess Hill, UK) and 1 mM dithiothreitol (DTT)) at 4 °C. Following centrifugation at 13 000 rpm for 8 min at 4 °C, cleared lysates were quantified for protein levels (Bradford). 300 μg of protein lysate was incubated with 20 μl of protein-G Sepharose beads and Ref-1 antibody (1:100) over-night at 4 °C with rotation, then washed 3 times with lysis buffer. Immunoprecipitated protein bound to beads were then solubilised in ×1 NuPAGE LDS sample buffer (Invitrogen, Paisley, UK) with 25 mm DTT and boiled at 70 °C for 10 min.

2.3. Western Blotting

Cell protein lysates and immunoprecipitated protein samples were subjected to sodium dodecyl sulphate–polyacrylamide gel electrophoresis using 12 lane NuPage pre-cast gels (Life Technologies/ThermoFisher Scientific, Waltham, MA, USA). Proteins were transferred to polyvinylidene difluoride membranes (Millipore, Edinburgh, UK), which were then blocked in 5 % (w/v) dry milk powder in Tris-buffered saline with 0.1 % (v/v) Tween. Blots were probed sequentially with primary antibodies overnight (1:1000) and then with horse radish peroxidase-conjugated secondary antibodies (1:10,000) with washing with Tris-buffered saline with 0.1 % (v/v) Tween. Enhanced Chemiluminescent solution was used to detect protein bands with hyperfilm (both GE Healthcare, Buckinghamshire, UK). All western blots are representative of at least three independent experiments. Processing of images were carried out using ImageJ. 1.43v, where background levels were removed by a small adjustment of contrast and brightness levels only.

2.4. Anchorage Independent Cell Growth in Soft Agar

6-well plastic tissue culture plates were coated with melted 0.6 % (w/v) agar in phosphate buffer saline. On top of this bottom layer after setting at room temperature, either MEFs (50,000 cells) or AML 621-101 (12,000 cells) as single cells were resuspended in melted 0.3 % (w/v) agar phosphate buffer saline with 50 % (v/v) Dulbecco's modified Eagle's medium supplemented at 40 °C. The top agar/cell layer was set in a 37 °C humidified tissue culture incubator. Working drug concentrations of each drug were set up within each layer prior to plating. 2 ml of media was added with working concentrations of each drug or DMSO (vehicle). Plates were grown for 4 weeks, with media and drug replaced twice weekly, before pictures were taken. Colony diameter was determined using ImageJ. (v.50) and colony numbers was scored.
6-well plastic tissue culture plates were coated with melted 0.6 % (w/v) agar in phosphate buffer saline. On top of this bottom layer after setting at room temperature, either MEFs (50,000 cells) or AML 621-101 (12,000 cells) as single cells were resuspended in melted 0.3 % (w/v) agar phosphate buffer saline with 50 % (v/v) Dulbecco's modified Eagle's medium supplemented at 40 °C. The top agar/cell layer was set in a 37 °C humidified tissue culture incubator. Working drug concentrations of each drug were set up within each layer prior to plating. 2 ml of media was added with working concentrations of each drug or DMSO (vehicle). Plates were grown for 4 weeks, with media and drug replaced twice weekly, before pictures were taken. Colony diameter was determined using ImageJ. (v.50) and colony numbers was scored.

2.5. Vasculature Mimicry

96-well tissue culture plate were coated with 50 µl chilled Matrigel (Growth factor reduced, LDEV-free) basement membrane matrix (Corning Inc., New York, USA) and were set at room temperature. Either 30,000 *Tsc2*−/− MEF cells or 50,000 AML 621-101 cells were resuspended in reduced-serum Optimem media (Life Technologies, Thermo Fisher Scientific, Waltham, MA, USA) and added to each coated well. Cells were treated with specified drugs or vehicle only and then placed in a hypoxic incubator. After 16 h, pictures were taken on an EVOS XL Core camera that we then analysed on ImageJ. using AngioTool software.

2.6. Cytotoxcity assays: Assays for Spheroids and Outgrowth and Acridine Orange/Propidium Iodide (AO/PI) Cell Viability

Spheroid formation and outgrowth analysis were performed as previously described [18]. Spheroids and cell outgrowth was imaged using a EVOS XL Core camera and then analyzed using ImageJ v1.50i. Cell viability was assessed using AO/PI stain reagent following the manufactures guidelines (Labtech, East Sussex, UK). Cells mixed with AO/PI were analysed on a LUNA-FL™ Dual Fluorescence Cell Counter.

2.7. Transcription Assays

Inducible luciferase reporter constructs for HIF-1α, STAT3 and NF-κB were purchased from Affymetrix Inc. (Milan, Italy). Transfections were carried out using JETPei (VWR International, Leicestershire, UK) using the manufacturer's protocol. Promega dual-luciferase reporter assay system was used in accordance with the manufacturer's protocol (Promega, Southampton, UK) using 20 µl of protein lysate. Luminescence was measured and standardised for protein content.

2.8. mRNA Expression

mRNA was preserved in cells using 0.5 ml RNAprotect Cell Reagent (Qiagen, West Sussex, UK). RNeasy Plus mini kit was used to extract mRNA using Qiashredders (purchased from Qiagen, West Sussex, UK) as described in the manufacturer's protocol. 1 µg mRNA from each sample was transcribed into cDNA using a Quantitect reverse transcription kit (Qiagen, West Sussex, UK) in a thermal cycler (Applied Biosystems, Carlsbad, CA, USA). All primer sets were

purchased from Qiagen. Quantitative real-time PCR reactions were conducted in 96-well plates using Sybr Green PCR Master mix and primers purchased from Qiagen (West Sussex, UK). Assays were performed: initial denaturation step (95 °C, 15 min), 40 cycles of denaturation (94 °C, 15 s), annealing step (55 °C, 30 s) and extension step (72 °C, 40 s). Amplification products were quantified during the fortieth cycle extension step. The ddCT (delta-delta-Ct) method was used and normalized to β-actin. Dissociation steps were performed to verify primer set specificity. Correct PCR amplicon size was verified by resolution on a 2 % polyacrylamide gel, 85 bp for Ref-1 (Catalogue number QT00094360) and 104 bp for β-actin (Catalogue number QT01680476). All Q-PCR primer assays were at least 96 % efficient.

2.9. Targeted Metabolic Profiling

To account for differences in cell size and protein content at harvest, *Tsc2*+/+ ($8x10^5$) and *Tsc2*−/− ($4x10^5$) MEFs were differentially seeded onto 10 cm^2 plates. The next day the cells were changed to 0.1 % (v/v) FBS DMEM and vehicle or 25 μM APX3330 were added ~6 h later. After overnight treatment, metabolites were extracted with ice cold high performance liquid chromatography (HPLC) grade 80 % (v/v) aqueous methanol from 5 replicate 10 cm^2 plates on dry ice as described previously [19]. Metabolites were processed and analyzed using selected reaction monitoring (SRM) with polarity switching on a 5500 QTRAP triple quadrupole mass spectrometer (AB/SCIEX) coupled to a Prominence UFLC HPLC system (Shimadzu) using amide hydrophilic interaction chromatography at pH 9.2. 296 endogenous water soluble metabolites were measured at steady-state (Metabolomics Core, Beth Israel Deaconess Medical Center, Boston, MA). The resulting raw metabolomics data were normalized to protein concentration of 3 additional replicate plates by multiplying a correction factor for each treatment group (calculated as mean total protein of all samples / mean total protein of group) and uploaded into MetaboAnalyst 3.0 (http://www.metaboanalyst.ca/MetaboAnalyst/) for subsequent processing and analysis. The peak area intensities for each metabolite were then normalized relative to vehicle treated *Tsc2*+/+ MEFs. Specifically, to generate processed data the peak areas were filtered by interquartile range and autoscaled (mean-centered and divide by the standard deviation for each variable) and Log^2 transformed and statistical analysis was applied to generate heatmaps and principal component analysis in MetaboAnalyst 3.0.

2.10. Oxygen Consumption and Extracellular Acidification Rate

Cells were seeded at $1x10^4$ cells per well in 100 μl 10 % (v/v) FBS DMEM and allowed to attach to the bottom of the assay plate. The cells were treated with vehicle or 2 μM APX3330 ~6 h later in 500 μl 10 % (v/v) FBS DMEM. The next day basal oxygen consumption rate and basal extracellular acidification rate were measured using a Seahorse Bioscience XF24 analyzer (Agilent, Santa Clara, CA, USA). The data were normalized by fixing the wells and staining with DAPI to quantify total nuclei per well.

2.11. Experimental repeats and statistical analysis

Experiments are representative of three experiments unless otherwise stated. Statistical analysis was carried out using GraphPad Prism 9, using multiple unpaired t-test or ANOVA when multiple comparisons were being carried out. One way ANOVA with Tukey's post hoc was used unless it was non-parametric data, which was instead analyzed with Kruskall-Wallis/Dunn's post hoc. In figures, p-value were represented as either < 0.05 *, < 0.01 **, < 0.001 ***, or as not significant 'NS'.

3. Results

3.1. Aberrant activation of HIF-1α/STAT3/NF-κB in Tsc2-deficient cells are restored with APX3330, a Ref-1 specific inhibitor

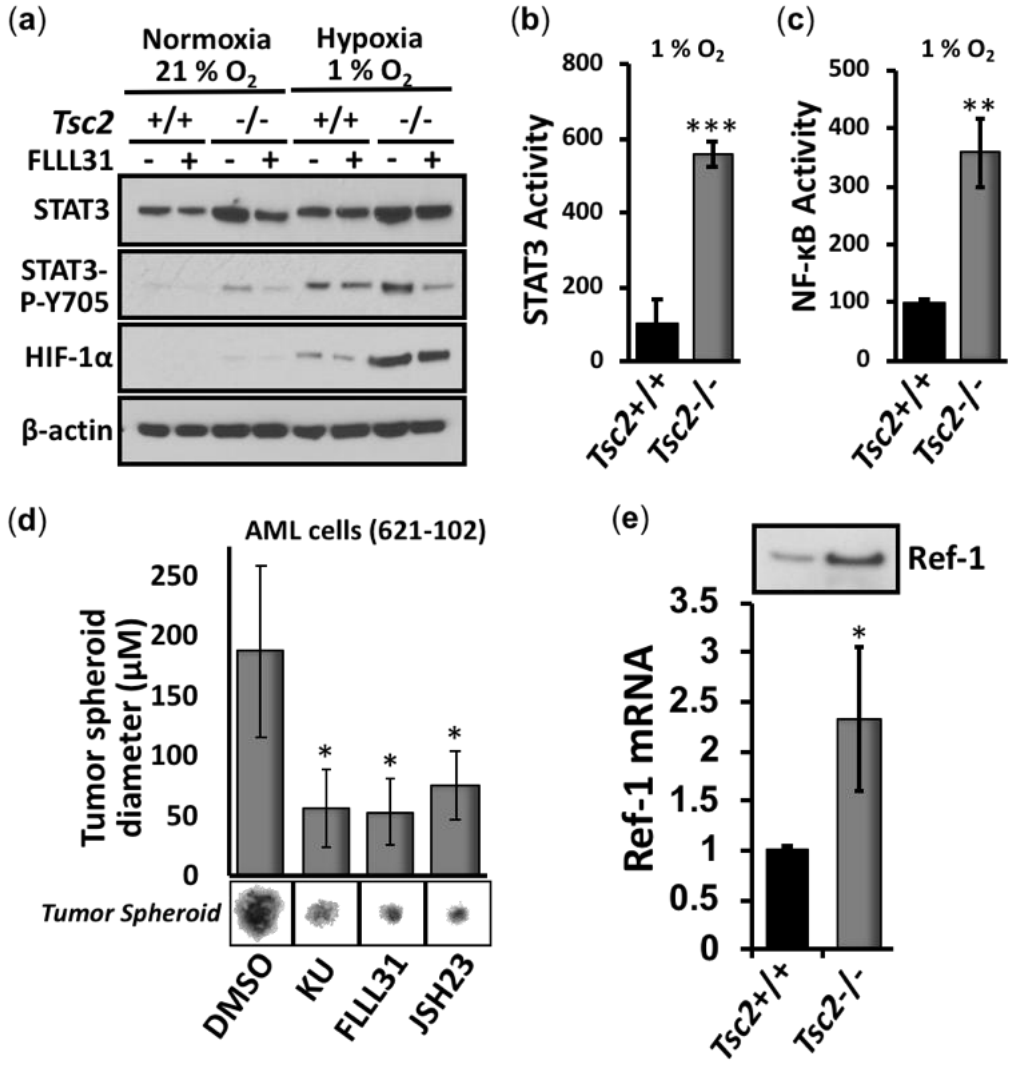

Initially, we compared STAT3 phosphorylation at Y705 and the protein levels of HIF-1α in *Tsc2*+/+ and *Tsc2*−/− MEFs under normoxia and hypoxia (Figure 1a). We observed a marked increase of Y705 phosphorylation of STAT3 and HIF-1α protein in the *Tsc2*−/− MEFs under hypoxia when compared to the wildtype *Tsc2*+/+ MEFs, showing that hypoxia causes an aberrant upregulation of these transcription factors in the absence of *Tsc2*. The STAT3 inhibitor, FLLL31 inhibited the hypoxic induction of STAT3 Y705 phosphorylation, but not the accumulation of HIF-1α protein. While it is known that loss of *TSC2* activates STAT3 [12-14], the degree of STAT3 hyperactivity in *TSC2*-deficient cells has not been quantified to date. Therefore, we carried out transcription assays on STAT3. We observed a marked elevation in the transcription activity of STAT3 (Figure 1b) in *Tsc2*−/− MEFs under hypoxia; over 3-fold induction when compared to the *Tsc2*+/+ wildtype controls. Similarly, the activity of another hypoxia-responsive transcription factor, NF-κB, was markedly upregulated in the *Tsc2*−/− MEFs under hypoxia when compared to wildtype *Tsc2*+/+ MEFs (Figure 1c). Our data indicates that hypoxic responsive transcription factors, such as HIF-1α, STAT3 and NF-κB become aberrantly activated when TSC2 is deficient.

Tumor formation assays were carried out in angiomyolipoma (AML) cells from a LAM patient (621-102) lacking functional TSC2 (Figure 1d). We find significant reduction in tumor diameter with the ATP competitive mTOR inhibitor (Ku-0063794), as expected. We also see significant reduction in tumor diameter with inhibitors for STAT3 and NF-κB inhibitor (FLLL31 and JSH23, respectively), showing that these transcription factors are likely involved in tumor growth.

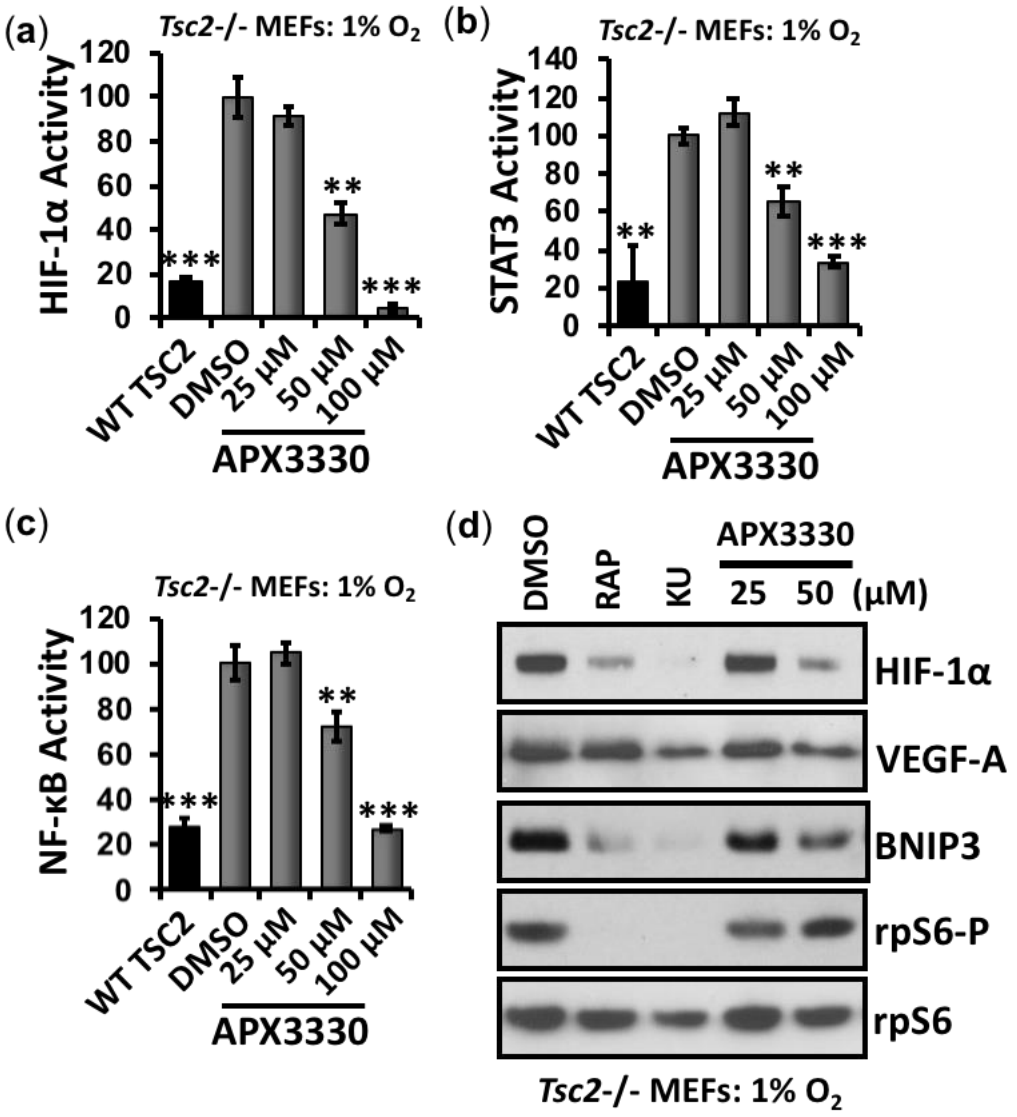

Given the above experimental evidence, we sought to find a therapeutic strategy where a single drug treatment might restore the activity of the three key hypoxic-responsive transcription factors STAT3, NF-κB and HIF-1α in TSC2-deficient cells. Fortuitously, Ref-1 is upstream of these transcription factors and has been shown to regulate their DNA binding activities through its redox function (reviewed in [16]). Ref-1 has two key functions in mammalian cells; DNA base excision repair activity and redox signaling. During conditions of redox stress, Ref-1 enhances the DNA-binding activity of multiple transcription factors, including HIF-1α, STAT3, and NF-κB, through reduction of critical cysteine residues within their DNA-binding or transactivation domains. To investigate the role that Ref-1 might play in promoting HIF-1α, STAT3, and NF-κB during hypoxia-mediated oxidative stress in TSC2, we first examined the levels of Ref-1 protein and mRNA. We observed at least 2-fold higher expression of Ref-1 in *Tsc2*−/− MEFs, when compared to wild-type controls (Figure 1e). To examine the effects of Ref-1 inhibition on these transcription factors in TSC, *Tsc2*−/− MEFs were treated with the specific Ref-1 inhibitor, APX3330, and the effects on transcriptional activity of HIF-1α (Figure 2a), STAT3 (Figure 2b),

and NF-κB (Figure 2c), was measured under hypoxia (1 % O_2). Of importance, APX3330 at 100 μM restored the aberrant activation of HIF-1α, STAT3 and NF-κB to a level comparable to cells re-expressing TSC2. At the lower 50 μM concentration, APX3330 treatment resulted in a significant reduction in the activity of HIF-1α, STAT3, and NF-κB.

Figure 2. APX3330 inhibits HIF-1α, STAT3 and NF-κB in *Tsc2*-deficient cells. *Tsc2*−/− MEFs were transiently transfected with (**a**) HIF-1α (**b**) STAT3 and (**c**) NF-κB luciferase vector with wild-type TSC2 vector (where indicated). Cells were subjected to hypoxia (1 % O_2) for 18 h in the presence of DMSO, or APX3330 (25, 50 and 100 μM) and transcription assays carried out, as indicated n=3. Error bars represent SD. ** p<0.01, *** p<0.001, compared to DMSO. (**d**) *Tsc2*−/− MEFs were treated with either DMSO, 50 nM rapamycin, 1 μM Ku-0063794 (KU) or APX3330 (25 or 50 μM) for 18 h under hypoxia (1 % O_2). Western blots for total HIF-1α, VEGF-A, BNIP3, and total and phosphorylated rpS6 were carried out, n=3.

Under hypoxia, 50 μM APX3330 was sufficient to reduce HIF-1α protein expression and downstream HIF-1α targets: VEGF-A and BNIP3 (Figure 2d). Unlike mTOR inhibition with either rapamycin or KU-006379, Ref-1 inhibition with APX3330 did not reduce ribosomal protein S6 (rpS6) phosphorylation. Therefore, the drug action of APX3330 to inhibit HIF-1α/VEGF-A/BNIP3 signaling is mTORC1-independent. Like rapamycin, APX3330 did not reduce STAT3-Y705 or RelA-S276 phosphorylation (Supplementary Figure S1), indicating that APX3330 inhibits DNA binding of these transcription factors, as is expected based on the redox function of Ref-1 [20]. Ref-1 presents as a new drug target for TSC (depicted in Figure 3), where Ref-1 inhibition functions as a different restorative therapy to the currently used mTOR inhibitors.

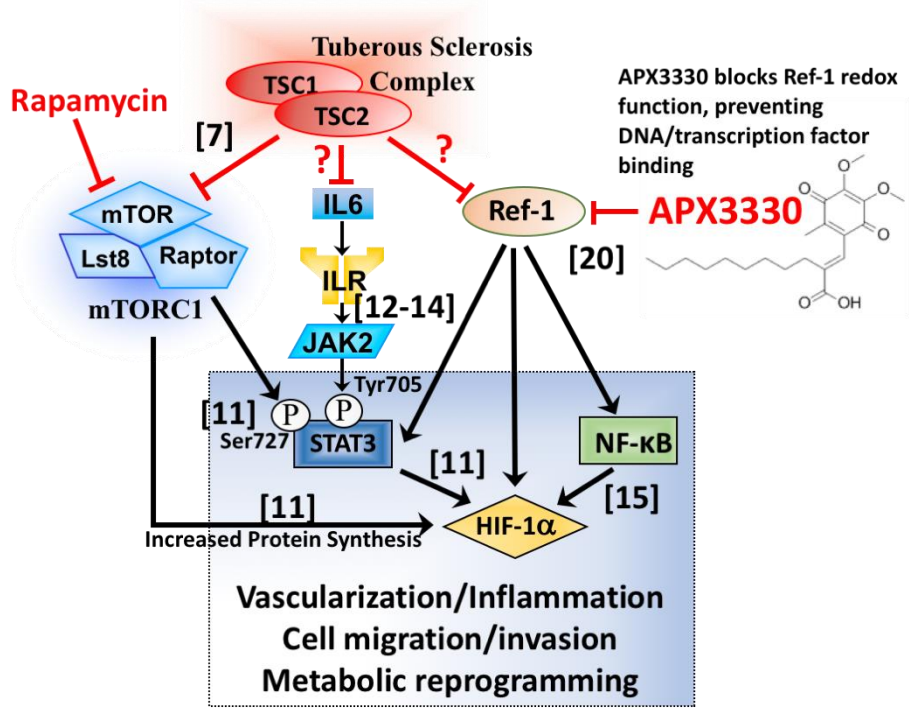

Figure 3. Diagram depicting Ref-1 redox signaling through STAT3, NF-κB and HIF-1α, a possible drug target for TSC. Multiple signaling inputs from TSC1/TSC2 towards STAT3 and HIF-1α are shown. References are imbedded in the figure revealing direct activatory or inhibitory signaling mechanisms. Both mTORC1-dependent and independent regulation towards STAT3, NF-κB and HIF-1α exist. This transcriptional node orchestrates vascularization, inflammation, cell migration/invasion, and metabolic

reprogramming. APX3330 blocks Ref-1 redox function to prevent interaction of these transcription factors with DNA.

3.2. APX3330 inhibits cell migration/invasion and tumor spheroid formation of Tsc2−/− MEFs

To explore whether Ref-1 inhibition has potency to revert other TSC-associated disease features, we carried out cell migration/invasion and tumor growth assays in *Tsc2*−/− MEFs after APX3330 treatment. At doses where HIF-1α, STAT3, and NF-κB are inhibited, APX3330 impaired wound closure of *Tsc2*−/− MEFs when compared to vehicle (Figure 4a).

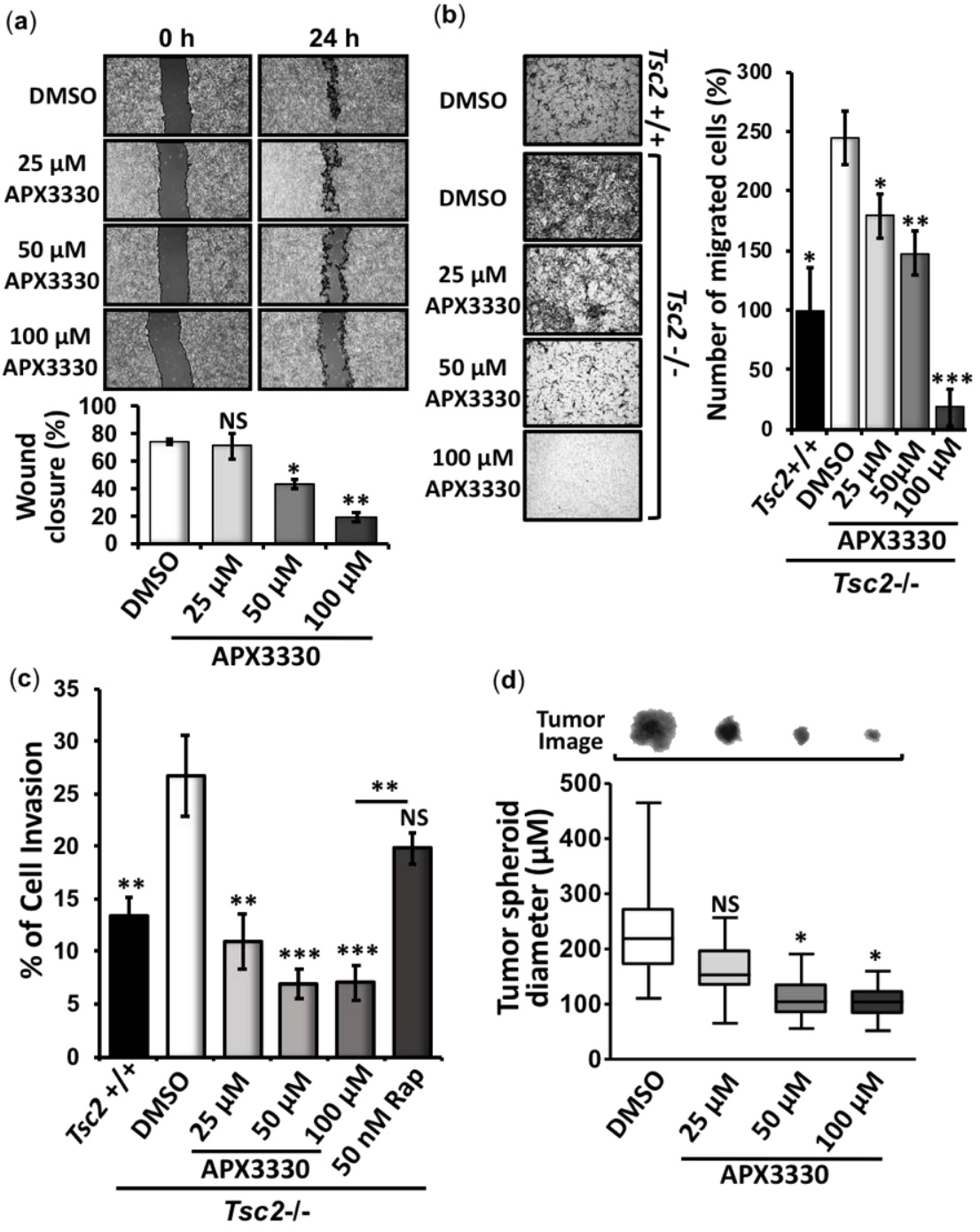

Figure 4. APX3330 inhibits cell migration/invasion and tumor formation of *Tsc2*−/− MEFs. *Tsc2*−/− MEFs were subjected to (**a**) wound scratch assays (*n*=3), (**b**) cell migration (*n*=3), (**c**) cell invasion (*n*=4),

and (**d**) *in vitro* tumor formation assays (30 tumors analyzed within 3 biological repeats) in the presence or absence of either DMSO or APX3330 (25, 50 and 100 μM), where indicated. *Tsc2*+/+ MEFs were used as controls in both the cell migration and cell invasion assays. Error bars represent SD (SEM for (d)), * p<0.05, ** p<0.01, *** p<0.001, when compared to DMSO.

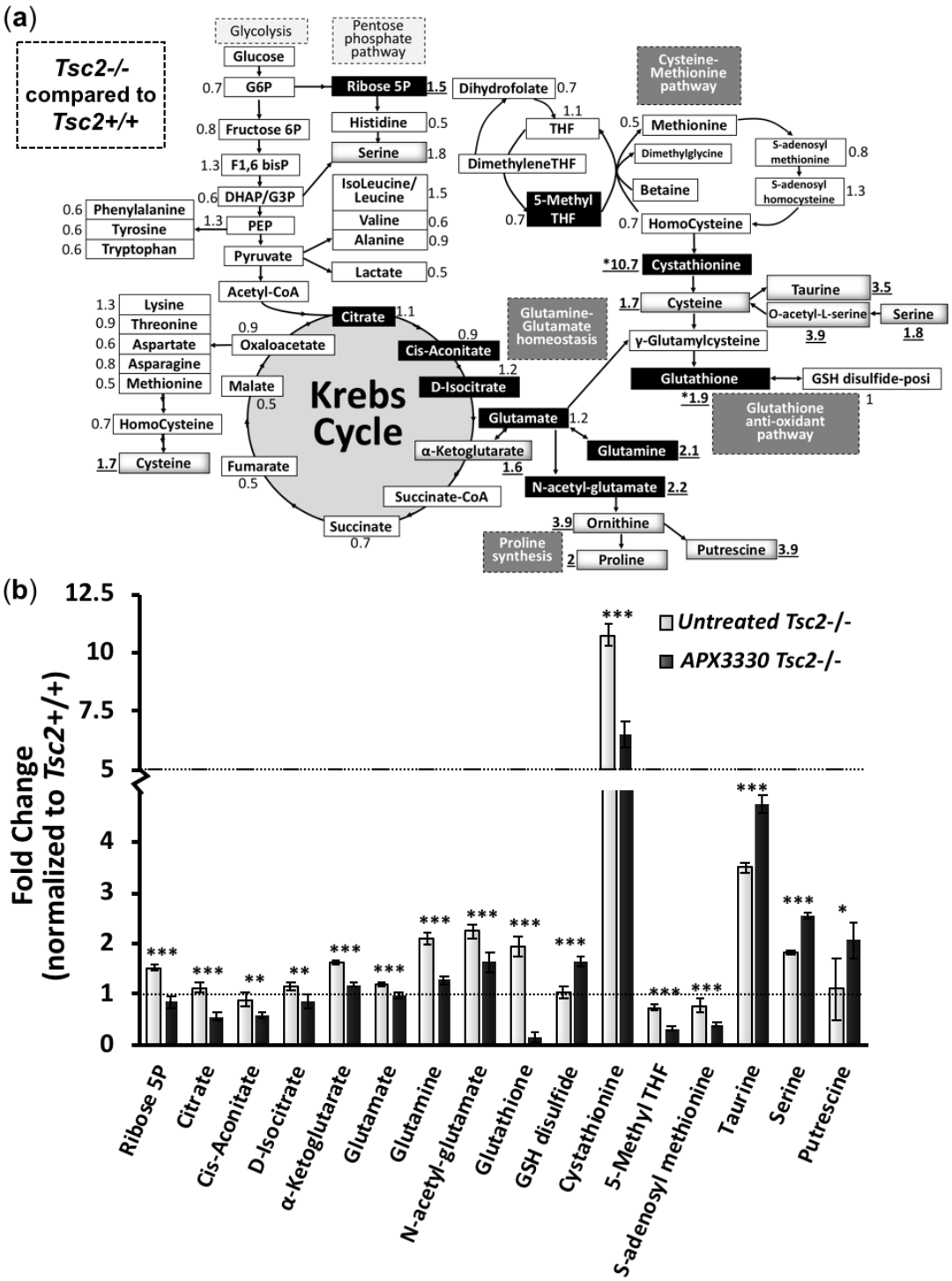

Figure 5. Metabolic profile of *Tsc2*−/− MEFs treated with APX3330 and compared to *Tsc2*+/+ MEFs. (**a**) *Tsc2*+/+ and *Tsc2*−/− (treated for 18 h with either DMSO or 25 μM APX3330 under serum-low conditions (0.1 % (v/v) FBS) were subjected to metabolomics, *n*=5. Metabolites are depicted and include: glycolysis, pentose phosphate pathway, Krebs cycle, cysteine-methionine pathway, glutamine-glutamate homeostasis, proline synthesis, and the glutathione anti-oxidant pathway. The values outside the metabolite boxes are the mean fold-change of the *Tsc2*−/− MEFs when compared to the *Tsc2*+/+ MEFs (where a value of 1 is equal between cells). Underlined are changes >1.5 fold, and cystathionine labelled with a * as the metabolite with the highest fold difference. Blackened boxes are metabolites that are reduced by APX3330. (**b**) Top scoring metabolites that are modulated by AX3330 are graphed, showing fold-changes of untreated and APX3330 treated *Tsc2*−/− MEFs normalized to untreated *Tsc2*+/+ MEFs. Error bars represent SD, * $p<0.05$, ** $p<0.01$, *** $p<0.001$, when comparing untreated versus APX3330 in Tsc2-/- MEFs.

3.3. Metabolic profiling shows restoration of redox homeostasis in the Tsc2−/− MEFs after APX3330 treatment

Metabolic profiles were determined in untreated *Tsc2*+/+ and *Tsc2*−/− MEFs, and APX3330 treated *Tsc2*−/− MEFs. Untreated *Tsc2*−/− MEFs were normalised to the untreated *Tsc2*+/+ controls and key changes in the metabolic profile between the untreated *Tsc2*−/− MEFs and normal untreated wild-type *Tsc2*+/+ MEFs are shown in Figure 5a. In the untreated *Tsc2*−/− MEFs, the Krebs cycle metabolite, α-ketoglutarate, was significantly higher when compared to *Tsc2*+/+ controls (elevated by 1.6-fold, Figure 5b). *Tsc2*−/− MEFs also had an elevated level of ribose-5-phosphate within the pentose phosphate pathway (PPP, elevated by 1.5-fold in the untreated *Tsc2*−/− MEFs versus the wild-type control), which is in line with previous reports that the PPP and *de novo* pyrimidine synthesis is upregulated in TSC2-deficient cells [21]. We also observed that untreated *Tsc2*−/− MEFs had a significantly higher level of glutamine, glutamate and N-acetyl-glutamate compared to wild-type. Of interest, APX3330 treatment was sufficient to reduce glutamine, glutamate and N-acetyl-glutamate in the *Tsc2*−/− MEFs. Glutamate, as well as cysteine, are essential metabolites in the generation glutathione (GSH), a tripeptide thiol antioxidant that was markedly elevated in the *Tsc2*−/− MEFs (1.9-fold increase) compared to wild-type. In cells, GSH is critically involved in antioxidant defense, typically involved in the reduction of H_2O_2 to generate H_2O and oxidized glutathione disulfide. The differential levels of GSH and glutathione disulfide in the untreated *Tsc2*−/− suggests oxidative stress. Other metabolites that can be biosynthetically derived from the amino acid glutamate were also observed to be elevated in the *Tsc2*−/− MEFs (when compared to wild-type) that included N-acetyl-glutamate (2.2-fold), ornithine (3.9-fold), proline (2-fold) and putrescine (3.9-fold). This data implies that TSC2-deficient cells have defects in proline synthesis. Supporting this observation, previous work has shown that TSC patients have a higher level of hydroxyproline in tumors and urine [22], and a higher level of free proline in blood [23].

A heat-map comparing the 3 samples, wild-type *Tsc2*+/+, untreated *Tsc2*−/− and APX3330 treated *Tsc2*−/− is shown in Supplementary S2A (normalised data, $n = 5$, can be found in Supplementary S3). Key differences between untreated and APX3330 treated *Tsc2*−/− MEFs are graphed in Figure 4b. APX3330 treatment reduced the levels of ribose-5-phosphate and Krebs cycle intermediates, citrate, cis-aconitate, D-isocitrate and α-ketoglutarate. Previous work showed that inhibition of Ref-1 redox activity blocked the cells' ability to utilize Krebs cycle substrates, α-ketoglutarate, succinate, fumarate, and malate [24]. Of interest, APX3330 dramatically reduced the levels of GSH and increased the levels of glutathione disulphide and cysteine, which infers that APX3330 treatment is impeding the generation of GSH and altering redox homeostasis. Ref-1 was previously described as having a redox chaperone activity, where Ref-1 regulated the DNA-binding activity of NF-κB through promoting reduction of the critical cysteine residues within NF-κB by other reducing molecules such as GSH and thioredoxin (Trx) [25]. Cysteine and GSH functions as two major cellular thiol antioxidants. Another potent thiol antioxidant and downstream metabolite of cysteine is the semi-essential non-proteinogenic amino acid, taurine, which was also observed to be significantly elevated in the *Tsc2*−/− MEFs when compared to the wild-type controls, and taurine was further enhanced with APX3330. The upstream

metabolite of cysteine, cystathionine, was upregulated in the *Tsc2*−/− MEFs (by 10.7-fold), and was reduced with APX3330 treatment. Other metabolites within the cysteine-methionine pathway, 5-methyl THF and S-adenosyl methionine, were also elevated in the *Tsc2*−/− MEFs, and reduced with APX3330. Proline and cysteine synthesis pathway intermediates appear to be favored in the Tsc2-/- MEFs, which could help explain why there is an elevated pool of reduced glutathione (GSH) (Figure 5a). GSH is a critical scavenger of reactive oxygen species (ROS). Consequently, the ratio of GSH with oxidised glutathione disulphide can be used as a marker of oxidative stress. The ratio of GSH:GSH disulphide is dramatically altered with APX3330 treatment (Figure 6a, with a ratio of 1:12 with APX3330). This shows that APX3330 is causing oxidative stress to the Tsc2-/- MEFs.

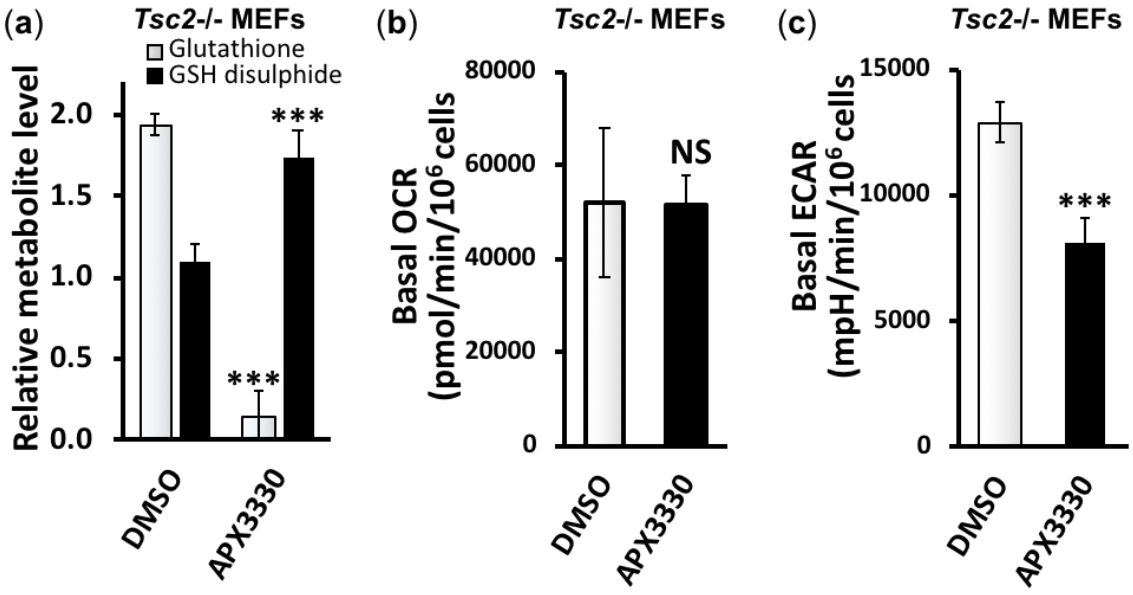

Figure 6. APX3330 treatment affects glutathione homeostasis and ECAR but not OCR. (**a**) The levels of glutathione and glutathione disulphide in the *Tsc2*−/− MEFs untreated and 25 μM APX3330 treated are graphed. (**b**) Basal oxygen consumption rate (OCR) and **(c)** extracellular acidification rate (ECAR) assessed in *Tsc2*−/− MEFs after 18 h treatment of 25 μM APX3330 in 10 % (v/v) FBS and compared to DMSO. Error bars represent SD, *** $p<0.001$, when compared to their paired DMSO control.

We next examined oxygen consumption (Figure 6b) and extracellular acidification rates (Figure 6c). While we observed that APX3330 did not change the oxygen consumption rates of the *Tsc2*−/− MEFs, APX3330 treatment dramatically reduced extracellular acidification rates. Extracellular acidification is linked to HIF-1α activation and lactic acid secretion that occurs during non-aerobic respiration. These results are in line with previous research, where APX3330 was found to reduce both HIF-1α activity via carbonic anhydrase IX (CAIX) and intracellular pH in pancreatic cancer cells [26]. In summary, APX3330 treatment reduced non-aerobic respiration, restored glutamine-glutamate homeostasis and altered the balance of antioxidant metabolites linked to the regeneration of GSH in the *Tsc2*−/− MEFs.

3.4. Second generation Ref-1 inhibitor, APX2009, shows increased potency to inhibit HIF-1α

Compared to APX3330, the second-generation inhibitor, APX2009, has increased potency to inhibit Ref-1 in various cancer cell models [26,27]. We compared the drug activity of rapamycin, APX3330 and APX2009 alone and in combination on HIF-1α activity by carrying out HIF-1α

transcriptional activity assays in *Tsc2*−/− MEFs subjected to hypoxia (Figure 7). At 100 μM, APX3330 inhibited HIF-1α by 90%, while rapamycin only reduced the activity of HIF-1α by 40%. Combination of APX3330 at 25 μM with rapamycin showed greater inhibition of HIF-1α, when compared to single drug treatments. As expected, we observed greater potency to inhibit HIF-1α with APX2009 when compared to treatment with the parental drug, APX3330, or with rapamycin alone. At 10 μM, APX2009 restored HIF-1α activity to a level equivalent to TSC2 re-expression. We observed no additional effects on HIF-1α activity when rapamycin was combined with APX2009. Treatment with RN7-58 (at 100 μM) was used as a negative control drug, as this modified APX2009 analogue is unable to act as a Ref-1 redox inhibitor [28]. As expected, RN7-58 did not inhibit the hypoxic induction of HIF-1α activity.

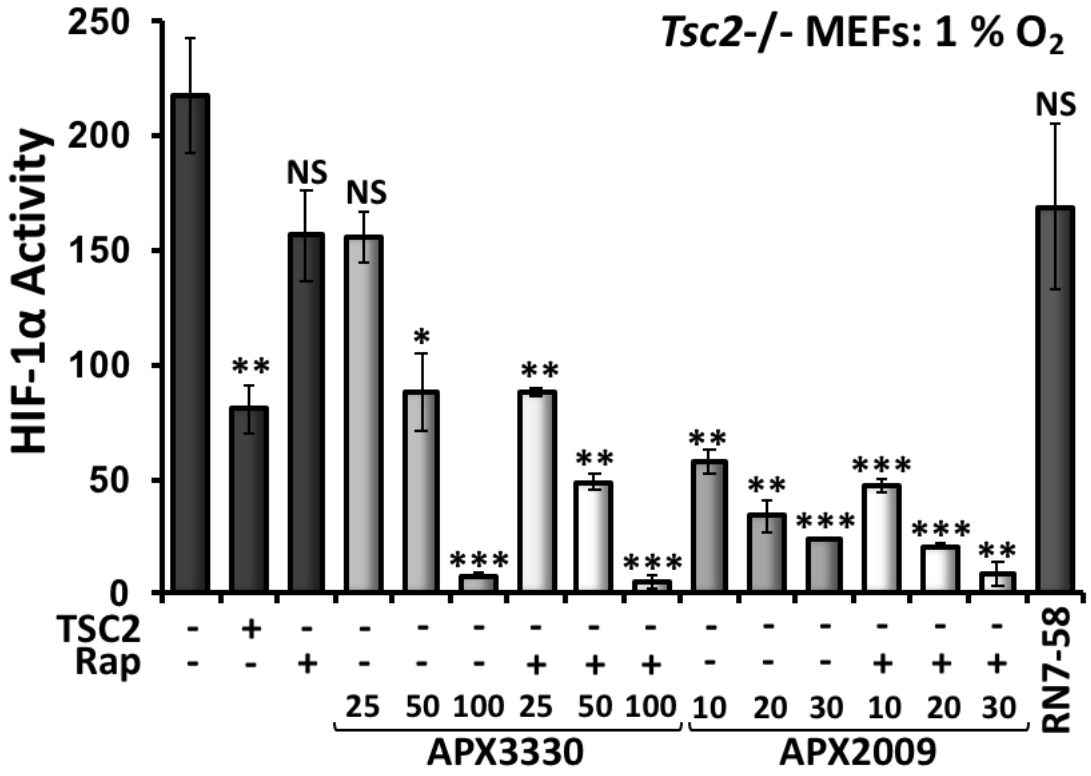

Figure 7. The second generation Ref-1 inhibitor, APX2009, potently inhibits HIF-1α while rapamycin was less effective. *Tsc2*−/− MEFs were transiently transfected with the HIF-1α luciferase vector (and TSC2/pcDNA3.1 vector as a control, where indicated). These cells were subjected to hypoxia (1 % O_2) for 18 h in the presence or either DMSO, 50 nM rapamycin, APX3330 (25, 50 and 100 μM) or APX2009 (10, 20 and 30 μM) or 100 μM of RN7-58 (control drug) as single agents or, where indicated, rapamycin was combined with APX3330 and APX2009. Luciferase assays to determine HIF-1α activity were carried out (*n*=3). Error bars represent SD, * p<0.05, ** p<0.01, *** p<0.001, when compared to untreated DMSO control.

3.5. Second generation Ref-1 inhibitors, APX2009 and APX2014 inhibit in vitro tumor growth of AML (621-102) cells

We next wanted to assess the anti-tumor activity of Ref-1 inhibitors in a LAM-patient angiomyolipoma derived cell line (621-102 AML cells) that lacks functional TSC2. We compared the activity of APX3330 with two second-generation inhibitors, APX2009 and APX2014, and mTOR inhibitors, rapamycin and Ku-0063794. We grew 621-102 AML cells in soft agar in the presence and absence of drug and determined the diameter of the tumor spheroids. Both mTOR inhibitors, rapamycin and Ku-0063794, were effective at reducing tumor diameter (Figure 8a). Upon comparison of Ku-0063794 and rapamycin, the number of tumor spheroids was decreased after treatment with Ku-

0063794, indicating that more complete inhibition of mTOR with the ATPase competitive inhibitor prevents colony formation. 621-102 AML cells require 15 % (v/v) FBS to form colonies in these *in vitro* tumor formation assays in soft agar. We saw that APX3330 was less effective at reducing the diameter of tumor spheroids (Supplementary Figure S2b), and likely reflects the higher levels of serum used in these assays. In line with this result, we observe less effectiveness of APX3330 with increasing serum concentrations (data not shown) due to the binding of APX3330 to serum proteins impacting its activity. However, in the presence of 15 % (v/v) FBS, the second generation inhibitors, APX2009 (at 10 and 20 μM) and APX2014 (at 5, 10 and 20 μM), showed enhanced potency to inhibit the number of tumor spheroids that grew (Figure 8a). With APX2009 and APX2014 treatment, there is a significant reduction in colony number. To further confirm inhibition of HIF-1α, the total protein levels of HIF-1α and its downstream target, BNIP3 were analysed in 621-102 AML cells and *Tsc2*−/− MEFs (Figure 8b). Second generation Ref-1 inhibitors (APX2009 and APX2014) were effective at reducing either HIF-1α or BNIP3 protein levels, while APX3330 was not, again demonstrating increased potency with new analogues. As previously observed in the *Tsc2*−/− MEFs, the Ref-1 inhibitors did not inhibit mTORC1 in the 621-102 AML cells, as observed by the high levels of rpS6-P after treatment.

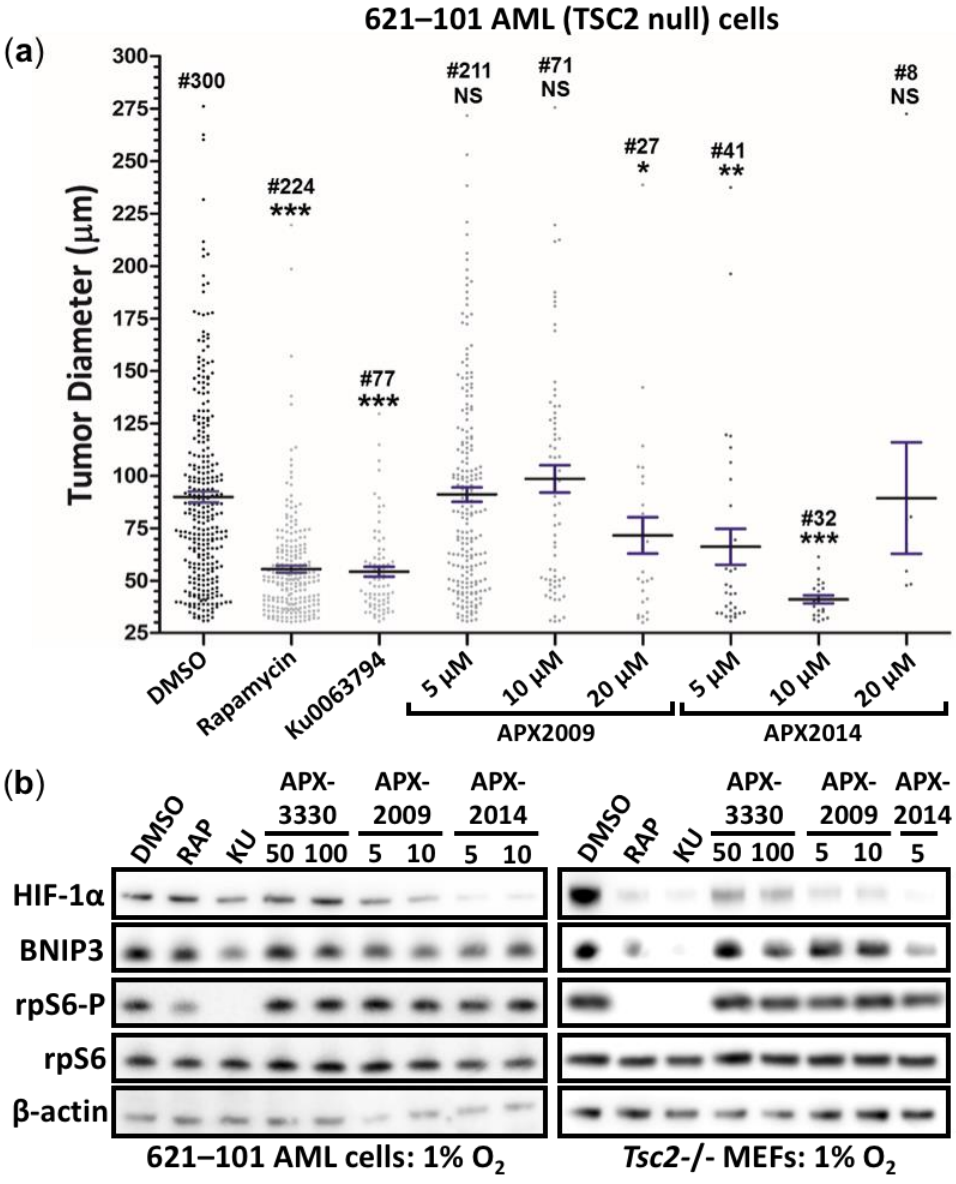

Figure 8. APX2009 and APX2014 show potency to inhibit *in vitro* tumor growth of 621-102 AML cells. (**a**) 621-102 AML cells were subjected to *in vitro* tumor formation assays in the presence or absence of either DMSO, 50 nM rapamycin, 1 μM Ku0063794, APX2009 (5, 10 and 20 μM) or APX2014 (5, 10 and 20 μM), where indicated. Tumor diameter was quantified; the numbers of tumors quantified are indicated above each column (up to 100 tumors analyzed within 3 biological repeats). Error bars represent SEM, * $p<0.05$, ** $p<0.01$, *** $p<0.001$, when compared to untreated DMSO control. (**b**) 621-102 AML cells (left panel) or *Tsc2*−/− MEFs (right panel) were treated with either DMSO, 50 nM rapamycin, 1 μM Ku-0063794 (KU), APX3330 (50 or 100 μM), APX2009 (5 or 10 μM), or APX2014 (5 or 10 μM), where indicated, for 18 h under hypoxia (1 % O_2). From prepared lysates, western blots for total HIF-1α, BNIP3, total and phosphorylated rpS6, and β-actin were carried out, n=3.

To determine whether the drugs had cytotoxic activity, we treated cell spheroids grown on soft agar (*Tsc2*-/- MEFs and 621-102 AML cells) with either DMSO, APX3330 (50 or 100 μM), APX2009 (5 or 10 μM), APX2014 (5 or 10 μM) or a known cytotoxic agent, etoposide (10 μM) for 11 days in the presence of serum. We then examined whether cells recovered treatment by transferring the cell spheroids to standard plastic coated tissue culture plates in the absence of drug. Both the *Tsc2*-/- MEFs and 621-102 AML cells recovered after treatment with either APX3330, APX2009 or APX2014 (similar to the DMSO control), as observed by cells migrating out of the adhered spheroid within a 48 h period (Supplementary Figure S4). No migrating cells were observed after etoposide treatment, showing cytotoxic activity as expected. Acridine orange/propidium iodide cell viability assays showed no loss of cell viability with APX3330 (50 or 100 μM), APX2009 (5 μM) or APX2014 (5 μM) in both *Tsc2*-/- MEFs and 621-102 AML cells, while some loss of cell viability became apparent using the higher APX2014 concentration of 10 μM (data not shown). Given the limited observed cytotoxicity, the drug activity of APX3330, APX2009 and APX2014 to impair migration, invasion, tumor formation and transcriptional activity are unlikely through drug cytotoxicity.

3.6. Vasculature mimicry was blocked with APX3330, APX2009 and APX2014, while mTOR inhibition was ineffective

During oxidative stress, we hypothesise that Ref-1 activates the STAT3/NF-κB/HIF-1α transcriptional signaling nexus to orchestrate a transcriptional programme to drive mTORC1-independent disease aspects of TSC. Based on the sensitivity of Ref-1 inhibitors to block STAT3 and HIF-1α activity, we reasoned that Ref-1 inhibition could impact the angiogenesis pathways in TSC. To explore this, we carried out vasculature mimicry assays. *Tsc2*−/− MEFs (Figure 9a) or 621-102 AML cells (Figure 9b) were grown under hypoxia on matrigel to encourage tube formation. Under hypoxia, both the *Tsc2*−/− MEFs and 621-102 AML cells form a tubular network that represents early stages of blood vessel vascularization. Of interest, inhibition of either Ref-1 with either APX3330, APX2009 and APX2014 was sufficient to inhibit vasculature mimicry in both the *Tsc2*−/− MEFs and 621-102 AML cells, while mTORC1 inhibition with rapamycin was not effective at the doses analyzed. A significant decrease was observed in average vessel length after Ref-1 inhibitor treatment with APX3330, APX2009 and APX2014, but not rapamycin (Figure 9a and 9b). Our data implies that mTORC1 inhibition is not sufficient to block hypoxia-induced vascularization of these TSC2-deficient cells, while blockade of redox signal transduction through Ref-1 is effective. This complements and supports what was previously observed in ocular studies and inhibition of angiogenesis

[29-32]. This data highlights that targeting Ref-1 could possibly have additional benefits to TSC patients to block tumor angiogenesis when compared to current therapies with mTORC1 inhibitors.

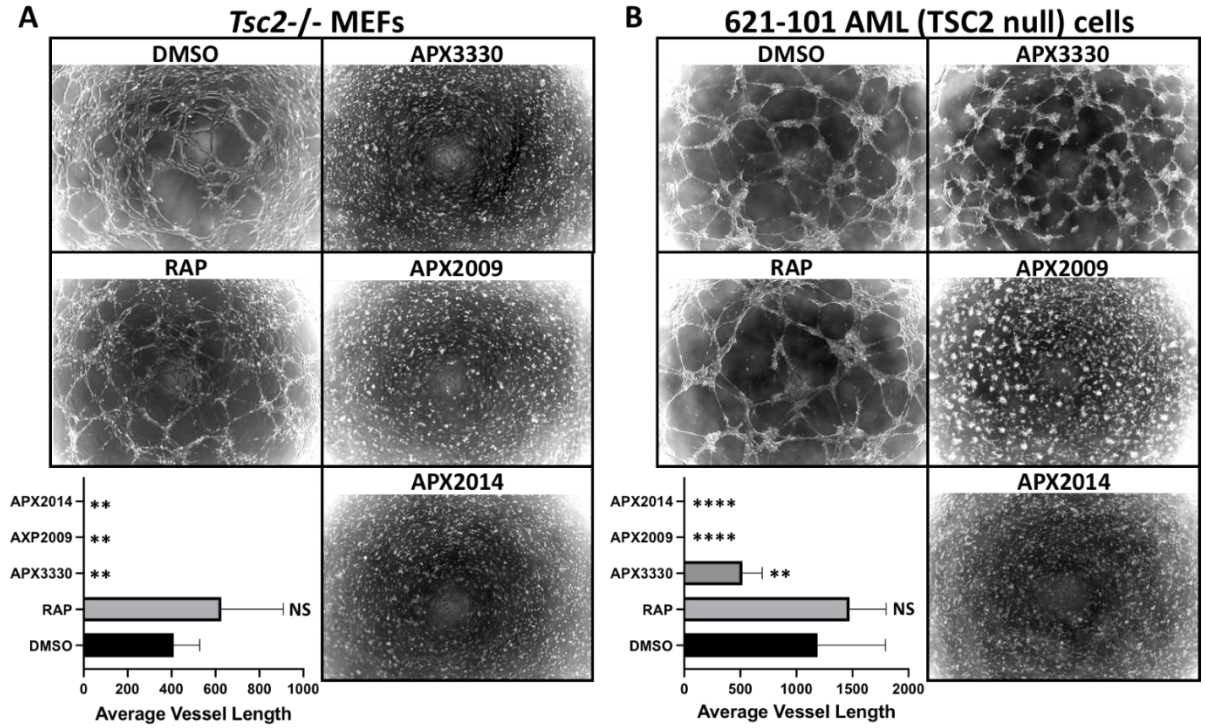

Figure 9. Ref-1 inhibitors block vasculature mimicry, while rapamycin was ineffective. Vasculature mimicry assays were carried out on (**a**) *Tsc2*−/− MEFs and (**b**) 621-102 AML cells on matrigel under hypoxia (1 % O_2) in the presence of either DMSO, 50 nM rapamycin, 50 μM APX3330, 5 μM APX2009 or 5 uM APX2014, (*n*=5). Average vessel length was quantified using AngioTool. One-way ANOVA with Tukey's multiple comparisons was carried out, not significant (NS), ** $p<0.01$, **** $p<0.0001$, when compared to untreated DMSO

4. Discussion

During conditions of oxidative stress, Ref-1 positively regulates redox-sensitive transcription factors, STAT3, NF-κB and HIF-1α to orchestrate a transcriptional programme to drive angiogenesis, metabolic transformation, and cell migration/invasion. These are critical disease facets of TSC and LAM that are not fully restored with mTOR inhibitors, and could help explain why we observe a stable but partial response with mTOR inhibitors in the clinical setting [9]. Therefore, Ref-1 and downstream redox-sensitive transcription factors regulated by Ref-1 present as new therapeutic targets. Importantly, our work indicates that Ref-1 inhibition might restore disease aspects of TSC linked to hypoxia and redox imbalance, processes that are less sensitive to mTOR inhibition. Furthermore, our work reveals that Ref-1 inhibition does not induce a selective cytotoxic response in the diseased cells.

We demonstrate that Ref-1 regulates the transcriptional activity of HIF-1α, STAT3 and NF-κB, which are aberrantly elevated in TSC2-deficient cells. Furthermore, Ref-1 inhibition potently blocked the migration and invasion of *TSC2*-deficient cells. It is worth noting, Ref-1 inhibition with APX3330 was more effective than rapamycin to block *Tsc2*−/− MEF cell invasion. This finding indicates that the metastatic traits of TSC2-deficient cells could be dependent on Ref-1-redox signaling, involving downstream transcription factors, such as STAT3. STAT3 is a key driver of metastasis in many cancers (for review see [33]). Therefore, our work highlights STAT3 as a possible drug target for the malignant

characteristics of TSC-associated LAM (and see [6]). The Ref-1/HIF-1α/STAT3/NF-κB signaling node likely contributes to disease attributes linked to TSC pathology, such as inflammation, cell migration/invasion, tumor growth, metabolic transformation and angiogenesis. The ability that Ref-1 inhibition can simultaneously impact multiple transcription factors makes Ref-1 an attractive drug target for the treatment of TSC.

APX3330 is more than a tool compound, as demonstrated by the results of our phase I APX3330 trial in solid tumors (Clinical Trials Identifier: NCT03375086). We observed a 30% response rate, RECIST partial response (PR), no significant toxicities, disease stabilization in six patients with four on drug for an extended time (252, 337, 357, and 421 days), predicted PK and target engagement based on patient biopsies showing a decrease in genes regulated by transcription factors regulated by Ref-1, such as HIF-1α, NF-κB and STAT3 [34,35]. We also observed patient serum levels of APX3330 between 50 and 130 μM, such that the doses presented here are within achievable levels in humans. APX3330 is also showing a strong safety profile in the ongoing Phase 2b diabetic retinopathy (DR)/diabetic macular edema (DME) clinical trial (unpublished data). However, second generation APX compounds as shown here are based on a robust SAR (structure activity relationship) program and have been identified and are beginning to be studied in various models including cancer [26,36], anti-ocular [32] disease models for age related macular degeneration [37] as well as inflammatory bowel disease (IBD). These studies included both the use of APX2009 and APX2014, which showed greater effect at lower drug concentrations and are nearing pre-IND enabling status.

Metabolic profiling revealed interesting differences between the *Tsc2*−/− MEFs and the wild-type controls. Upon loss of *Tsc2*, metabolites involved in glutamine metabolism were markedly different, implicating possible changes to glutamine-dependent purine synthesis, redox homeostasis, and energy metabolism. Glutamate is a precursor for regenerating antioxidant metabolites, such as GSH. The shift in the metabolic profile to favor glutamate could have disease implications in neurons of TSC patients. This is because, α-ketoglutarate is transaminated along with glutamine to form the excitatory neurotransmitter glutamate. Indeed, abnormalities in glutamate homeostasis has been linked to seizure frequency in TSC-models [38]. Therefore, restoring glutamine/glutamate metabolism with APX3330, and additional analogues, might have potential benefits in *TSC2*-deficient cells.

5. Conclusions

In TSC2-deficient cells, Ref-1 functions as an important redox-sensor that turns on an array of redox-sensitive transcription factors, such as STAT3, HIF-1α, and NF-κB. Through these transcription factors, Ref-1 promotes angiogenesis, inflammation and metabolic transformation that further supports tumor growth of TSC2-deficient cells. The activity of Ref-1 is not mediated through mTORC1. Therefore, this Ref-1 redox sensitive pathway presents itself as a potential therapeutic target to treat disease aspects of TSC that may have additional benefits to mTORC1 inhibitors alone.

Supplementary Materials: The following are available online at http://www.mdpi.com/**ADD**, Figure S1: APX3330 does not reduce RelA S276 or STAT3 Y705 phosphorylation in *Tsc2*−/− MEFs; Figure S2: heatmap of metabolite data on *Tsc2*+/+ and *Tsc2*−/− MEFs and tumor formation assay in 621-102 AML cells treated with APX3330; S3 file: normalised data for metabolomic data presented in Figure 4; Figure S4: *Tsc2*−/− MEFs and 621-102 AML tumor spheroids recover after Ref-1 inhibitor treatment in an outgrowth assay.

Author Contributions: Conceptualization, A.R.T.; Investigation, J.D.C., K.M.D., H.C.L., M.A.M.A., S.S., E.R., D.O.S, and A.R.T.; Resources, M.R.K., B.C., and A.R.T.; Data Curation, J.D.C., K.M.D. and A.R.T.; Methodology, J.D.C., K.M.D., H.C.L. and E.P.H.; Formal Analysis, J.D.C., K.M.D., H.C.L. and A.R.T.; Writing-Original Draft Preparation, A.R.T.; Writing-Review & Editing, H.C.L., M.L.F.; M.R.K. and A.R.T.; Supervision, A.A., E.P.H., D.M.D., A.R.T.; Project Administration, A.R.T.; Funding Acquisition, A.R.T and K.M.D.

Funding: Research was funded by the TS Association (2013-F02 to K.M.D. and A.R.T, and 2018-S04 to J.C. and A.R.T.), King Fahd Security College / Ministry of Interior / Saudi Arabia (ref: 1050795978 to M.A.M.A. and A.R.T.). M.R.K. and M.L.F. were supported by grants from the National Institute of Health and National Cancer Institute R01CA167291 and R01CA254110. M.R.K. was also supported by NIH/NCI grants R01CA205166, R01CA231267, R01EY031939 and R01HL140961. M.L.F was supported by NIH/NCI grant U01HL143403, R01CA211098 and R01NF180045. M.L.F. and M.R.K. were additionally supported by the Riley Children's Foundation and the IU Simon Comprehensive Cancer Center, P30CA082709.

Acknowledgments: We would like to thank Min Yan and John Asara, PhD of the Mass Spectrometry Core, Beth Israel Lahey Health/Beth Israel Deaconess Medical Center, Boston, MA for assistance with metabolomics.

Conflicts of Interest: The authors declare no conflict of interest. Mark R. Kelley has licensed APX3330 through Indiana University Research and Technology Corporation to Apexian Pharmaceuticals LLC. APX2009 and APX2014 are second generation compounds from Apexian Pharmaceuticals. APX3330 has been licensed to Ocuphire Pharma from Apexian Pharmaceuticals for eye diseases and diabetes. Neither Apexian Pharmaceuticals, nor Ocuphir Pharma had neither control nor oversight of the studies, interpretation, or presentation of the data in this manuscript.

References

1. McEneaney, L.J.; Tee, A.R. Finding a cure for tuberous sclerosis complex: From genetics through to targeted drug therapies. In *Advances in Genetics*; Kumar, D., Ed.; Elsevier: New York, USA, 2019; Volume 103, pp. 91–118. doi: 10.1016/bs.adgen.2018.11.003
2. Henske, E.P.; Jóźwiak, S.; Kingswood, J.C.; Sampson, J.R.; Thiele, E.A. Tuberous sclerosis complex. *Nat. Rev. Dis. Primers.* **2016,** *2*, 16035. doi: 10.1038/nrdp.2016.35
3. Pirson, Y. Tuberous sclerosis complex-associated kidney angiomyolipoma: from contemplation to action. *Nephrol. Dial. Transplant* **2013**, *28*, 1680–1685. doi: 10.1093/ndt/gft009
4. Wang, S.; Fallah A. Optimal management of seizures associated with tuberous sclerosis complex: current and emerging options. *Neuropsychiatr. Dis. Treat*. **2014**, *10*, 2021–2030. doi: 10.2147/NDT.S51789
5. Henske, E.P.; McCormack, F.X. Lymphangioleiomyomatosis - a wolf in sheep's clothing. *J. Clin. Invest*. **2012,** *122*, 3807–3816. doi:10.1172/JCI58709
6. Carsillo, T.; Astrinidis, A.; Henske, E.P. Mutations in the tuberous sclerosis complex gene TSC2 are a cause of sporadic pulmonary lymphangioleiomyomatosis. *Proc. Natl. Acad. Sci. U.S.A*. **2000**, *97*, 6085–6090. doi:10.1073/pnas.97.11.6085
7. Tee, A.R.; Manning, B.D.; Roux, P.P.; Cantley, L.C.; Blenis, J. Tuberous sclerosis complex gene products, Tuberin and Hamartin, control mTOR signaling by acting as a GTPase-activating protein complex toward Rheb. *Curr. Biol*. **2003**, *13*, 1259–1268. doi: 10.1016/s0960-9822(03)00506-2
8. Rad, E.; Murray, J.T.; Tee, A.R. Oncogenic Signalling through Mechanistic Target of Rapamycin (mTOR): A Driver of Metabolic Transformation and Cancer Progression. *Cancers* **2018**, *10*, 5. doi: 10.3390/cancers10010005
9. Bissler, J.J.; McCormack, F.X.; Young, L.R.; Elwing, J.M.; Chuck, G.; Leonard, J.M,; Schmithorst, V.J.; Laor, T.; Brody, A.S,; Bean, J.; Salisbury, S.; Franz, D.N. Sirolimus for angiomyolipoma in tuberous sclerosis complex or lymphangioleiomyomatosis. *N. Engl. J. Med*. **2008**, *358*, 140–151. doi: 10.1056/NEJMoa063564
10. Brugarolas, J.B.; Vazquez, F.; Reddy, A.; Sellers, W.R.; Kaelin, W.G.Jr. TSC2 regulates VEGF through mTOR-dependent and -independent pathways. *Cancer Cell* **2003**, *4*, 147–158. doi: 10.1016/s1535-6108(03)00187-9.

11. Dodd, K.M.; Yang, J.; Shen, M.H.; Sampson, J.R.; Tee, A.R. mTORC1 drives HIF-1α and VEGF-A signalling via multiple mechanisms involving 4E-BP1, S6K1 and STAT3. *Oncogene* **2015**, *34*, 2239–2250. doi: 10.1038/onc.2014.164.
12. Magri, L.; Cambiaghi, M.; Cominelli, M.; Alfaro-Cervello, C.; Cursi, M.; Pala, M.; Bulfone, A.; Garcìa-Verdugo, J.M.; Leocani, L.; Minicucci, F.; Poliani, P.L.; Galli, R. Sustained activation of mTOR pathway in embryonic neural stem cells leads to development of tuberous sclerosis complex-associated lesions. *Cell Stem Cell* **2011**, *9*, 447–462. doi: 10.1016/j.stem.2011.09.008
13. Himes, B.E.; Obraztsova, K.; Lian, L.; Shumyatcher, M.; Rue, R.; Atochina-Vasserman, E.N.; Hur, S.K.; Bartolomei, M.S.; Evans, J.F.; Krymskaya, V.P. Rapamycin-independent IGF2 expression in Tsc2-null mouse embryo fibroblasts and human lymphangioleiomyomatosis cells. *PLoS One* **2018**, *13*, e0197105. doi: 10.1371/journal.pone.0197105
14. Weichhart, T.; Costantino, G.; Poglitsch, M.; Rosner, M.; Zeyda, M.; Stuhlmeier, K.M.; Kolbe, T.; Stulnig, T.M.; Hörl, W.H.; Hengstschläger, M.; Müller, M.; Säemann, M.D. The TSC-mTOR signaling pathway regulates the innate inflammatory response. *Immunity* **2008**, *29*, 565–577. doi: 10.1016/j.immuni.2008.08.012
15. van Uden, P.; Kenneth, N.S.; Rocha, S. Regulation of hypoxia-inducible factor-1alpha by NF-kappaB. *Biochem. J.* **2008**, *412*, 477–484. doi: 10.1042/BJ20080476
16. Mijit, M.; Caston, R.; Gampala, S.; Fishel, M.L.; Fehrenbacher, J.; Kelley, M. R. APE1/Ref-1 - One Target with Multiple Indications: Emerging Aspects and New Directions. *J. Cell. Signal.* **2021**, *2*, 151–161.
17. Yu, J.; Astrinidis, A.; Howard, S.; Henske, E.P. Estradiol and tamoxifen stimulate LAM-associated angiomyolipoma cell growth and activate both genomic and nongenomic signaling pathways. *Am. J. Physiol. Lung Cell Mol. Physiol.* **2004**, *286*, L694–L700. doi: 10.1152/ajplung.00204.2003
18. Dunlop, E.A.; Johnson, C.E.; Wiltshire, M.; Errington, R.J.; Tee, A.R. Targeting protein homeostasis with nelfinavir/salinomycin dual therapy effectively induces death of mTORC1 hyperactive cells. *Oncotarget* **2017**, *8*, 48711-48724. doi.org/10.1038/s41388-018-0381-2
19. Parkhitko, A.A.; Priolo, C.; Coloff, J. L.; Yun, J.; Wu, J.J.; Mizumura, K.; Xu, W.; Malinowska, I.A.; Yu, J.; Kwiatkowski, D.J.; Locasale, J.W.; Asara, J.M.; Choi, A.M.; Finkel, T.; Henske, E.P. Autophagy-dependent metabolic reprogramming sensitizes TSC2-deficient cells to the antimetabolite 6-aminonicotinamide. *Mol. Cancer Res.* **2014**, *12*, 48–57. doi.org/10.1158/1541-7786.MCR-13-0258-T
20. Cardoso, A.A.; Jiang, Y.; Luo, M.; Reed, A.M.; Shahda, S.; He, Y.; Maitra, A.; Kelley, M. R.; Fishel, M.L. APE1/Ref-1 regulates STAT3 transcriptional activity and APE1/Ref-1-STAT3 dual-targeting effectively inhibits pancreatic cancer cell survival. *PLoS One* **2012**, *7*, e47462. doi.org/10.1371/journal.pone.0047462
21. Ben-Sahra, I.; Howell, J.J.; Asara, J.M.; Manning, B.D. Stimulation of *de novo* pyrimidine synthesis by growth signaling through mTOR and S6K1. *Science* **2013**, *339*, 1323–1328. doi: 10.1126/science.1228792
22. Tanaka, H.; Arima, M. tuberous sclerosis: hydroxyproline content in urine and tissues. *Brain Dev.* **1981**, *3*, 81–85. doi.org/10.1016/s0387-7604(81)80009-5
23. Tanaka, H.; Nakazawa, K.; Arima, M.; Morooka, K.; Suzuki, F.; Aoki, T.; Kohno, Y. Tuberous sclerosis: proline and hydroxyproline contents in serum. *Brain Dev.* **1983**, *5*, 450–456. doi.org/10.1016/s0387-7604(83)80073-4
24. Gampala, S.; Shah, F.; Lu, X., Moon; H. R., Babb; O., Umesh Ganesh; N., Sandusky, G.; Hulsey, E.; Armstrong, L.; Mosely, A. L.; Han, B.; Ivan, M.; Yeh, J. J.; Kelley, M. R.; Zhang, C.; Fishel, M. L. Ref-1 redox activity alters cancer cell metabolism in pancreatic cancer: exploiting this novel finding as a potential target. *J. Exp. Clin. Cancer Res.* **2021**, *40*, 251. doi.org/10.1186/s13046-021-02046-x
25. Ando, K.; Hirao, S.; Kabe, Y.; Ogura, Y.; Sato, I.; Yamaguchi, Y.; Wada, T.; Handa, H. A new APE1/Ref-1-dependent pathway leading to reduction of NF-kappaB and AP-1, and activation of their DNA-binding activity. *Nucleic Acids Res.* **2008**, *36*, 4327–4336. doi: 10.1093/nar/gkn416

26. Logsdon, D.P.; Grimard, M.; Luo, M.; Shahda, S.; Jiang, Y.; Tong, Y.; Yu, Z.; Zyromski, N.; Schipani, E.; Carta, F.; Supuran, C.T.; Korc, M.; Ivan, M.; Kelley, M.R.; Fishel, M.L. Regulation of HIF1α under Hypoxia by APE1/Ref-1 Impacts CA9 Expression: Dual Targeting in Patient-Derived 3D Pancreatic Cancer Models. *Mol. Cancer Ther.* **2016**, *15*, 2722–2732. doi: 10.1158/1535-7163.MCT-16-0253
27. McIlwain, D.W.; Fishel, M.L.; Boos, A.; Kelley, M.R.; Jerde, T.J. APE1/Ref-1 redox-specific inhibition decreases survivin protein levels and induces cell cycle arrest in prostate cancer cells. *Oncotarget* **2017**, *9*, 10962–10977. doi: 10.18632/oncotarget.23493
28. Kelley, M.R.; Luo, M.; Reed, A.; Su, D.; Delaplane, S.; Borch, R.F.; Nyland, R.L.; 2nd, Gross, M.L.; Georgiadis, M.M. Functional analysis of novel analogues of E3330 that block the redox signaling activity of the multifunctional AP endonuclease/redox signaling enzyme APE1/Ref-1. *Antioxid. Redox Signal.* **2011**, *14*, 1387–1401. doi: org/10.1089/ars.2010.3410
29. Jiang, A.; Gao, H.; Kelley, M.R.; Qiao, X. Inhibition of APE1/Ref-1 redox activity with APX3330 blocks retinal angiogenesis *in vitro* and *in vivo*. *Vision Res.* **2011**, *51*, 93–100. doi: 10.1016/j.visres.2010.10.008
30. Li, Y.; Liu, X.; Zhou, T.; Kelley, M.R.; Edwards, P.; Gao, H.; Qiao, X. Inhibition of APE1/Ref-1 redox activity rescues human retinal pigment epithelial cells from oxidative stress and reduces choroidal neovascularization. *Redox Biol.* **2014**, *2*, 485–494. doi: 10.1016/j.redox.2014.01.023
31. Li, Y.; Liu, X.; Zhou, T.; Kelley, M.R.; Edwards, P.A.; Gao, H.; Qiao, X. Suppression of choroidal neovascularization through inhibition of APE1/Ref-1 redox activity. *Investig. Ophthalmol. Vis. Sci.* **2014**, *55*, 4461–4469. doi: 10.1167/iovs.14-14451
32. Sardar Pasha, S.; Sishtla, K.; Sulaiman, R.S.; Park, B.; Shetty, T.; Shah, F.; Fishel, M.L.; Wikel, J.H.; Kelley, M.R.; Corson, T.W. Ref-1/APE1 Inhibition with Novel Small Molecules Blocks Ocular Neovascularization. *J. Pharmacol. Exp. Ther.* **2018**, *367*, 108–118. doi: 10.1124/jpet.118.248088
33. Kamran, M.Z.; Patil, P.; Gude, R.P. Role of STAT3 in cancer metastasis and translational advances. *BioMed Res. Int.* **2013**, 421821. doi: org/10.1155/2013/421821
34. Chu, L.; Anderson, A.K.L.; Landers, M.A.; Wang, Y.; Kelley, M.R.; Messmann, R.A. CTC enumeration and characterization as a pharmacodynamic marker in the phase I clinical study of APX3330, an APE1/Ref-1 inhibitor, in patients with advanced solid tumors. *J. Clin. Oncol.* **2019**, *37*, e14531–e14531 doi: 10.1200/JCO.2019.37.15_suppl.e14531
35. Shahda, S,; Lakhani, N.J; O'Neil, B.; Rasco, D.W.; Wan, J.; Mosley, A.L.; Liu, H.; Kelley, M.R.; Messmann R.A. A phase I study of the APE1 protein inhibitor APX3330 in patients with advanced solid tumors. *J. Clin. Oncol.* **2019**, *37*, 3097–3097 doi: 10.1200/JCO.2019.37.15_suppl.3097
36. Fishel, M. L., Xia, H., McGeown, J., McIlwain, D. W., Elbanna, M., Craft, A. A., Kaimakliotis, H. Z., Sandusky, G. E., Zhang, C., Pili, R., Kelley, M. R., & Jerde, T. J. (2019). Antitumor Activity and Mechanistic Characterization of APE1/Ref-1 Inhibitors in Bladder Cancer. *Mol. Cancer Ther.* **2019**, *18*, 1947–1960. doi: 10.1158/1535-7163.MCT-18-1166
37. Kelley, M.R.; Wikel, J.H.; Guo, C.; Pollok, K.E.; Bailey, B.J.; Wireman, R.; Fishel, M.L.; Vasko, M.R. Identification and Characterization of New Chemical Entities Targeting Apurinic/Apyrimidinic Endonuclease 1 for the Prevention of Chemotherapy-Induced Peripheral Neuropathy. *J. Pharmacol. Exp. Ther.* **2016**, *359*, 300–309. doi: 10.1124/jpet.116.235283
35. Zeng, L.H.; Bero, A.W.; Zhang, B.; Holtzman, D.M.; Wong, M. Modulation of astrocyte glutamate transporters decreases seizures in a mouse model of Tuberous Sclerosis Complex. *Neurobiol. Dis.* **2010**, *37*, 764–771. doi: 10.1016/j.nbd.2009.12.020